Morphological Evolution and Ordered Quantum Structure Formation in Heteroepitaxial Core−Shell Nanowires

Jun-Yan Guo,[†,‡] Yong-Wei Zhang,[†,‡,*] and Vivek B. Shenoy[§,*]

[†]Department of Materials Science and Engineering, National University of Singapore, Singapore 117546, [‡]Institute of High Performance Computing, Fusionopolis, 1 Fusionopolis Way, #16-16, Connexis, Singapore 138632, and [§]School of Engineering, Brown University, 182 Hope Street, Providence, Rhode Island 02912

ABSTRACT We have performed three-dimensional dynamic simulations to study strain-driven morphological evolution and the formation of quantum structures on heteroepitaxial core−shell nanowire surfaces. Our simulations show that depending on geometric and material parameters, such as the radius of the wire, the thickness of the shell, and the mismatch strain, various surface morphologies including smooth core−shell nanowire surfaces, nanoring arrays, nanowire arrays, and ordered quantum dot arrays can be obtained by controlling initial surface configurations through prepatterning. It is also shown that these quantum structures may be trapped in a metastable state and may undergo a series of metastable state transitions during subsequent dynamic evolution. Our results identify possible pathways for fabrication of ordered quantum structures on the epitaxial core−shell nanowire surfaces and provide guidelines for achieving smooth core−shell structures.

KEYWORDS: core−shell nanowire · misfit strain · surface morphology · instability · quantum structures

Advances in synthesis and fabrication of coherently strained semiconductor heterostructures, such as quantum dots[1−3] (QDs) and core−shell nanowires,[4−7] offer the prospect for accurate and scalable device engineering at an atomistic scale for applications in electronics, photonics, and biology.[8] Since the optical and electronic properties of low-dimensional nanostructures are sensitive to morphology, dimension, composition, and, especially, strain, they can be "tuned" to very specific requirements. Thus, control of surface morphology and engineering of strain is of significant importance in fabrication of these structures. It has been recognized that the strain is crucial to the morphological evolution and growth of nanostructures. For example, stressed planar thin films are susceptible to formation of surface undulations or corrugations through surface diffusion driven by elastic strain energy. This phenomenon is often called the Asaro−Tiller−Grinfeld instability.[9−13] A useful consequence of the thin film surface instability is the formation of arrays of coherent 3D islands that spontaneously appear during the growth of strained films. This growth mode provides a natural route to fabricate quantum dot arrays in a number of different material systems.[14−16]

The morphological instability inherent to strained thin films has recently also been observed in strained core−shell nanowires. For example, experiments from Pan *et al.*[17] and Goldthorpe *et al.*[18] have revealed the growth of the 3D germanium (or silicon) islands around a silicon (or germanium) core during the growth of Si−Ge core−shell nanowires. While the understanding of the factors that control the morphological stability is important for growing smooth core−shell structures on the one hand, on the other hand, quantum dot arrays grown by this process can open up opportunities for novel photonic and electronic devices. For example, new energy levels that arise from the formation of quantum structures could be potentially exploited to allow more efficient absorption of solar energy in nanowire-based solar cells.[19] Most recently, Huang *et al.*[20] have experimentally obtained pure germanium QDs on both sides of ~20 nm thick, ~80 nm wide free-standing silicon nanoribbons *via* the Stranski−Krastanov growth or quantum dot self-assembly. This opens up a new way to create mechano-electronic superlattices.

Only a limited amount of work is currently available on the morphological stability of heteroepitaxial core−shell nanowires.[21,22] Schmidt and co-workers[21] performed an analysis of the stability of coherently strained core−shell nanowires using a first-order perturbation method. Their investigation showed the existence of a parameter range within which surface instabilities arise during growth. Very

*Address correspondence to zhangyw@ihpc.a-star.edu.sg, vivek_shenoy@brown.edu.

Received for review February 20, 2010 and accepted July 27, 2010.

Published online August 3, 2010. 10.1021/nn101218r

recently, Wang and co-workers[22] also used a similar linear perturbation analysis to study the morphological stability for epitaxial core−shell nanowires against various patterns of perturbation under conditions where mass transport occurs *via* surface diffusion or deposition growth kinetics. They studied the combined effect of geometric parameters such as core diameter and shell thickness and the inherited misfit strain on the morphology instability of epitaxial core−shell nanowires. It should be noted that since the above studies employ a small perturbation approximation in their first-order instability analyses, these results can only be used to study the early stage of surface evolution when the amplitudes of surface perturbations are small. The formation and coarsening of quantum dots and other nanostructures on a core−shell nanowire surface is well beyond the scope of the first-order instability analysis. Three-dimensional dynamic simulation methods that can handle strain relaxation due to surface features without making any approximations on their sizes and shapes are therefore needed for assessing the long-term stability and morphologies of core−shell structures. This understanding is necessary for controlling the surface morphology and hence guiding the fabrication of nanostructures such as nanorings or nanogrooves on nanowire surfaces.

In the present work, we have developed a three-dimensional dynamical simulation framework to study the formation of nanostructures on core−shell nanowires. We demonstrate that, depending on initial modes of perturbations and geometric parameters, different surface nanostructures can be obtained, including the smooth core−shell structure, nanoring arrays, nanowire arrays, and ordered quantum dot arrays. We further show that these regular nanostructures can be trapped in long-lived metastable states and can in principle undergo coarsening when subjected to further annealing. To gain control on surface morphology, prepatterning is commonly employed in planar thin film systems. Using our 3D simulations, we predict how patterns in core−shell systems influence the arrangement of nanostructures; we have identified particular patterns that can lead to highly ordered nanostructure arrays. Our results should therefore provide important guidance in determining material parameters for fabricating various surface quantum structures in core−shell nanowire systems.

RESULTS AND DISCUSSION

The configuration of the core−shell material system that we consider is schematically illustrated in Figure 1, where a core whose radius is R_c and the shell with a radius R_s are coherently bonded. As a result, the thin shell is initially uniformly strained in both circumferential and axial directions due to lattice misfit. The misfit strain is defined as $\varepsilon_m = (a_f - a_s)/a_s$, where a_f and a_s are lattice constants for the shell and the core lattices, respectively. When the system is in mechanical equilibrium, both the core and the shell are elastically strained.[21] For simplicity, the elastic properties such as shear modulus μ and Poisson's ratio ν are taken to be the same for both the core and the shell in the present study.

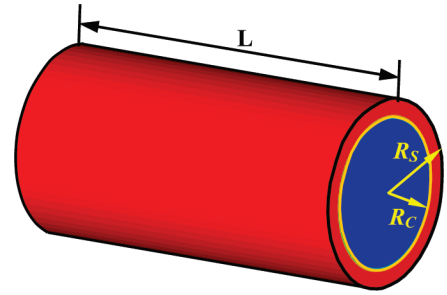

Figure 1. Schematic depiction of a core−shell nanowire. Here, *L* is the length of the nanowire, and R_c and R_s are the core and shell radii, respectively.

Figure 2 shows an instability map for a typical Ge/Si core−shell nanowire derived from linear stability analysis (refer to the Methods section). In this case, the misfit strain, Young's modulus, and Poisson's ratio are taken to be 4.2%, 80 GPa, and 0.3, respectively. The geometric parameters of the core−shell nanowire are chosen as follows: the outer radius $R_s = 3.3$ and the shell thickness $h = 0.3$, where the lengths are normalized by γ/ω_0, that is, the ratio of the surface energy of the shell and the strain energy density for a biaxial strained flat film. In all of the calculations we have carried out, the time scale is normalized by $t_0 = \gamma^3/(\Omega w_0^4 D)$. Ω is the atomic volume, $D = (\delta_s D_0/K_B T)e^{-Q_s/k_B T}$ is the mass diffusivity in diffusive layer, where $D_0 e^{-Q_s/k_B T}$ is the atomic diffusion coefficient; δ_s is the diffusion layer thickness; Q_s is the diffusion barrier; k_B is the Boltzmann constant; and T is the temperature, which is held at 900 K throughout the annealing. For the Ge/Si heteroepitaxial system at the annealing temperature, the units for length and time are 5.5 nm and 0.2 μs, respectively.

Since linear stability analysis employs a small perturbation approximation, that is, it assumes that the amplitudes of surface undulations are small, the above results can only be used to study the early stage of surface evolution. The formation and coarsening of fully formed quantum dots and other nanostructures on a core−shell nanowire surface is well beyond the scope of the linear instability analysis. Quantitative methods that can handle these nonlinear phenomena are therefore needed for *predicting* the long-term stability and morphologies of core−shell structures. As discussed in the Methods section, we have developed a finite element-based method that treats elastic fields accurately for any shape of surface perturbations without restrictions on their amplitude. Furthermore, the effect of the wetting layer, essential to treat the situations where surface perturbations grow in amplitude and reach the substrate, is also included in our 3D model.

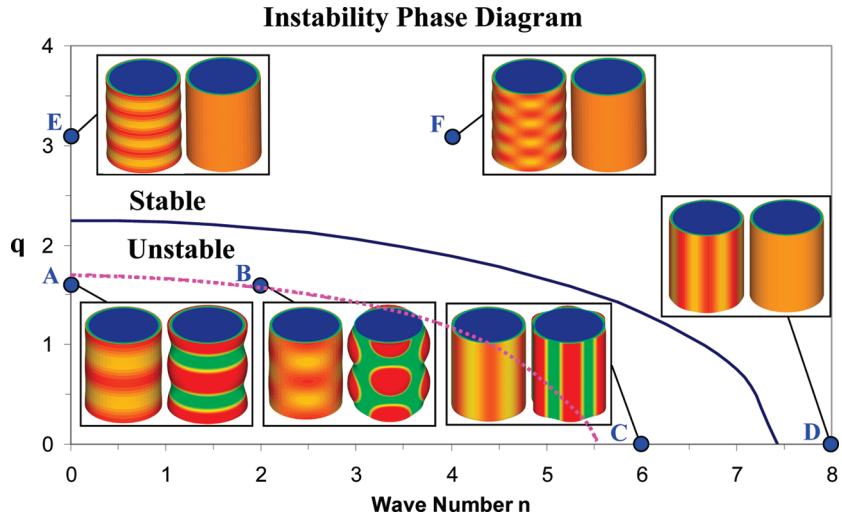

Figure 2. Instability map for a core−shell nanowire surface with shell radius $R_s = 3.3$, core radius $R_c = 3.0$, and a perturbation amplitude of 0.03 (around 1% of the radius). The solid dark blue curve is the boundary between the unstable and stable regions. The dotted pink curve is the fastest growth mode for the unstable growth regime. Wavenumbers n and q are $n = 0$ and $q = 1.56$ for point A; $n = 2$ and $q = 1.56$ for point B; $n = 6$ and $q = 0.0$ for point C; $n = 8$ and $q = 0.0$ for point D; $n = 0$ and $q = 3.12$ for point E; and $n = 4$ and $q = 3.12$ for point F. The left frame for each point shows the initial perturbation ($t = 0.0$), while the right one shows the first metastable state.

Next, we perform 3D dynamical simulations where the instability map in Figure 2 is employed as a useful reference for identifying the morphologies of interest.

In performing the dynamical simulations, we pick six perturbed modes (points A−F) on the map (Figure 2). Note that the initial perturbation modes to the core−shell nanowire surface for the points D, E, and F fall in the regime of stable perturbations, while the points A, B, and C are in the unstable regime. Therefore, for points D−F, these initial perturbations should decay with time according to the first-order perturbation result. The three-dimensional dynamical simulation results corresponding to points D, E, and F are shown in the insets of Figure 2. The initial perturbation amplitude is taken to be $\delta = 0.03$, which satisfies the small perturbation assumption in the linear instability analysis. It is seen clearly that all three perturbations decay as the surface evolves, in agreement with the first-order perturbation analysis. On the other hand, the perturbation modes at points A, B, and C fall in the unstable regime on the instability map. Point A corresponds to the initial perturbation along the axial direction only, that is, $n = 0$ and $q = 1.56$; point B corresponds to $n = 2$ and $q = 1.56$, and point C corresponds to the initial perturbation along the circumferential direction only, that is, $n = 6$ and $q = 0$. Also these modes are very close to the dashed line marking the fastest growth modes in Figure 2. We have found that all three perturbations grow with time. Inset A shows the growth of mode A. Here, the initial perturbation grows and quickly develops into a ring array. Inset B shows the growth of the perturbation mode B, leading to the formation of a well-arranged quantum dot array. Similarly, inset C also shows the growth of the perturbation mode C where the perturbed surface develops into an array of nanowires (or grooves) parallel to the axis of the core−shell nanowire. These calculations show that the first-order perturbation results are consistent with our three-dimensional dynamical simulations at the early stages of evolution. More interestingly, they also show that initial perturbations can be used to control the formation of various surface structures.

When initial perturbations grow in amplitude or when the film surface approaches the interface between the film and substrate, the linear perturbation method is no longer valid. Figure 3a shows our results for the evolution of the core−shell surface for the perturbation mode A as the amplitudes of the initial perturbation increase in magnitude. To understand the stability of different patterns that form during evolution, we have plotted the total strain energy in the system as a function of time in Figure 4. From this plot, it is seen that the strain energy decreases rapidly as the amplitude of the perturbation increases due to the formation of the nanoring array. Between $t = 2.0$ and 12.0, there is very little change in surface morphology which corresponds to the plateau region in Figure 4. After annealing for a longer duration, these nanorings break up into regular islands (see Figure 3a at $t = 18.0$). Formation of the islands leads to further relaxation of elastic energy, as seen in Figure 4. This island array is also metastable and can undergo further coarsening, leading to a regular array of islands arranged in two rows sitting symmetrically on opposite sides of the core−shell nanowire at $t = 54.0$. A similar phenomenon is also observed for the perturbation mode at point B. These regularly distributed islands formed at the early stage of growth (see Figure 3b at $t = 6.0$) are also in a metastable state (as evidenced by the plateau in Figure 4) and undergo coarsening when subjected to annealing.

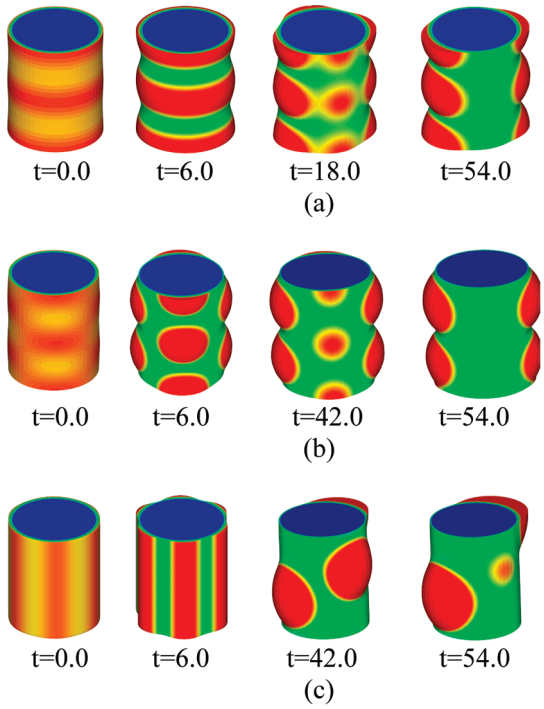

Figure 3. (a−c) Coarsening of strained islands for the three cases corresponding to points A (with $n = 0$ and $q = 1.56$), B ($n = 2$ and $q = 1.56$), and C ($n = 6$ and $q = 0.0$) indicated in Figure 2, respectively.

These islands evolve into a coarser, yet regularly distributed island array, as shown in Figure 3b at $t = 54.0$. Unlike the perturbations A and B, which are close to the fastest growing modes in Figure 2, case C is located in the unstable regime but far from the fastest growing modes. Therefore, the perturbations initially grow at a smaller rate, as seen from the relatively modest decrease in strain energy in Figure 4. However, subsequently the parallel surface nanowires formed at the early stage (see Figure 3c at $t = 6.0$) eventually break up into islands (see Figure 3c at $t = 42.0$). These islands sit at opposite sides of the core−shell nanowire and also undergo coarsening upon annealing (see Figure 3c at $t = 54.0$). (Refer to the Supporting Information Movie 1 and Movie 2, which clearly show the multiple metastable states formed at different stages of evolution.)

As demonstrated by our simulations (with different modes A, B, and C), different distributions of island arrays can be obtained by changing the nature of the initial perturbations. A different example considered is given in Figure 5, which shows the results of annealing a core−shell nanowire (the outer radius $R_s = 6$) with a helical surface perturbation. In the early stage, the relaxation of the strain energy provided by this perturbation is small (see Figure 4) since the nature of the surface undulations are qualitatively different from that of the fastest growing perturbations described in Figure 2. Here, the hill-tops of the initial helical perturbations grow into helical ridges around the core−shell nanowire (see Figure 5 at $t = 6.0$). This is a metastable state as evidenced from the plateau in the strain energy shown in Figure 4. Subsequently, the ridges break up into a helically distributed island array (see Figure 5 at $t = 18.0$). Note that, at this stage, this array provides very efficient relaxation of strain energy and is more favorable compared to all other perturbations considered in Figure 3. This array is also in a metastable state and undergoes further coarsening during annealing (see Figure 5 at $t = 54.0$). Clearly, the initial surface perturbations play an important role in the formation of surface morphology.

We have performed systematic three-dimensional dynamical simulations to understand the effect of random initial perturbations on the evolution of surface morphology. Figure 6 shows the snapshots of the evolution of a core−shell nanowire surface perturbed randomly. We find that the small wavelength components of the perturbation decay in magnitude while the wave components close to the fastest growth mode (Figure 2) grow in amplitude. As a consequence, the initial random surface breaks up into islands that are spaced at

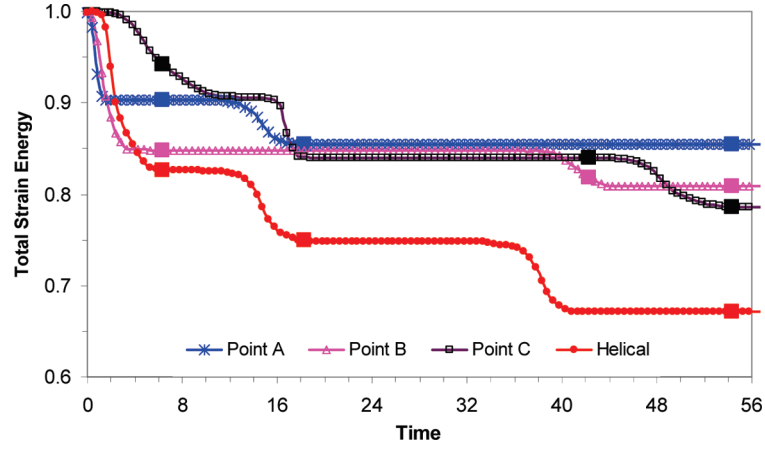

Figure 4. Total strain energy *versus* time for various initial perturbations in Figure 3 and Figure 5. The plateaus in these curves correspond to metastable configurations in the surface morphology. The snapshots in Figures 3 and 5 are marked by the filled squares in the curves.

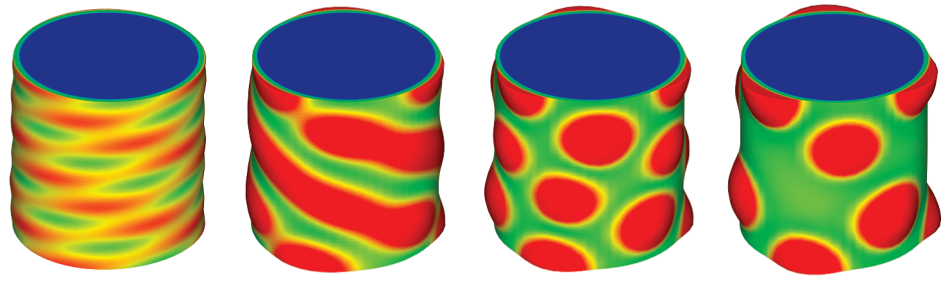

Figure 5. Morphological evolution of the surface of a core−shell nanowire (shell radius R_s = 6.3 and core radius R_c = 6.0) with an initial helical perturbation of amplitude of 0.03.

distances close to the fastest growth wavelength, indicating the tendency of the islands to self-assemble. Subsequently, islands with roughly the same size are left behind, on the opposite sides of the core−shell nanowire, as shown in Figure 6. It is important to note that this arrangement of islands is in qualitative agreement with experimental observations,[18] where the well-formed islands were found to align asymmetrically on opposite sides of the core−shell nanowire surface.

We have also investigated the effect of the variation of outer radius of the core−shell nanowire on the morphological instability of the core−shell nanowires. Figure 7 shows the instability maps of core−shell nanowires with the same shell thickness (taken to be 0.3) but different outer radii. We find that core−shell systems with smaller cores tend to be much more stable than the system with larger cores as the regime of unstable growth of wires with small cores shrinks significantly with the decrease of the outer radius of the nanowire. This is due to the fact that, as the core radius becomes smaller, the core is the more strained compared to the shell.[23,24] This is the reason why core−shell nanowires of small diameters are more suitable for obtaining smoother morphologies, as observed in experiments.[17,18]

Prepatterning methods have been adopted for guided growth of nanostructures on planar thin films, using either chemical and/or physical means.[25−30] In the present simulations, we assume that the surface prepatterning is performed by using direct writing techniques, such as electron beam lithography or scanning probe lithography. Scanning probe methods are capable of resolving surface features with subnanometer precision and creating patterns with atomic resolution, albeit at extremely slow speeds. Recently, nanoscale three-dimensional patterning of molecular resists using scanning probes has been realized, enabling the transfer of the pattern into arbitrary complex underlying substrates.[30] Hence it is expected that, in the near future, it would be possible to prepattern curved surfaces, such as nanowire surfaces, with nanometer resolution. Next, we perform three-dimensional dynamical simulations to understand the effect of prepatterning on the morphological evolution of the core−shell nanowire surface. Here, we consider a core−shell nanowire surface prepatterned with a pitch distance P_z along the axial direction and P_θ (angle) along the circumferential direction; the shape of the pattern is given by $H_0\cos(z\pi/z_0)\cos(\theta\pi/\theta_0)$, $-z_0 < z < z_0$ and $-\theta_0 < \theta < \theta_0$, where z and θ are the distance and angle along axial and circumferential directions from an island center, respectively. Thus $2z_0$ and $2\theta_0$ are the widths of the island along the two directions, and H_0 is the height of the island.

Figure 8 shows annealing of a surface with prepatterned island arrays with different pitches (the prepatterned islands are of the same size). Upon annealing, the evolutions of the prepatterned island arrays with P_z = 4.0 and $P_\theta = 2\pi/n$ (n varies from 1 to 5) are shown in Figure 8a−e, respectively. For cases c and d, where n = 3 and 4, respectively, a one-to-one relation between the prepatterned islands and the growing islands is retained during the annealing process. This is due to the fact that the spacings of the prepatterned is-

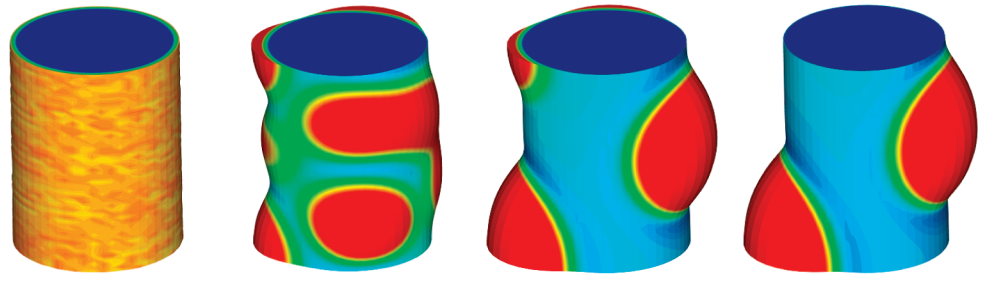

Figure 6. Morphological evolution of a randomly perturbed surface of a core−shell nanowire. The shell radius is R_s = 3.3, the core radius R_c = 3.0, and the perturbation amplitude 0.03 (around 1% of the radius).

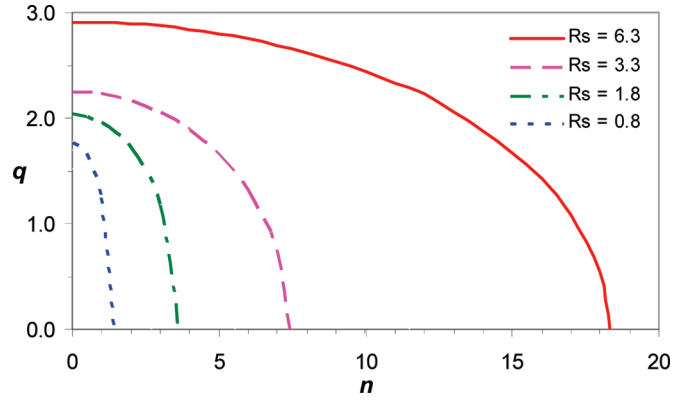

Figure 7. Effect of variation of the outer radius on the instability of a core−shell nanowire surface. A decrease in the outer radius leads to the decrease in the domain of instability.

land array are comparable with that of the fastest growth modes (see Figure 2). The ordering of the array of islands is found to remain stable with time, indicating that the prepatterning can prevent island coarsening. For case a, where the circumferential pitch is large ($P_\theta = 2\pi$), there is no one-to-one relation between the prepatterned islands and the formed dots. If $P_\theta = \pi$ (see $t = 0.0$ in Figure 8b), initially there is no one-to-one relationship (see $t = 3.0$ in Figure 8b); however, the newly formed dots disappear when subjected to further annealing (see $t = 6.0$ and 9.0 in Figure 8b) and the one-to-one relation is recovered. For case e, where the pitch in circumferential direction is small, $P_\theta = 2\pi/5$, that is, the islands come closer to each other along this direction (see $t = 0.0$ in Figure 8e), the initial prepatterned array of islands evolves into nanoring structures when

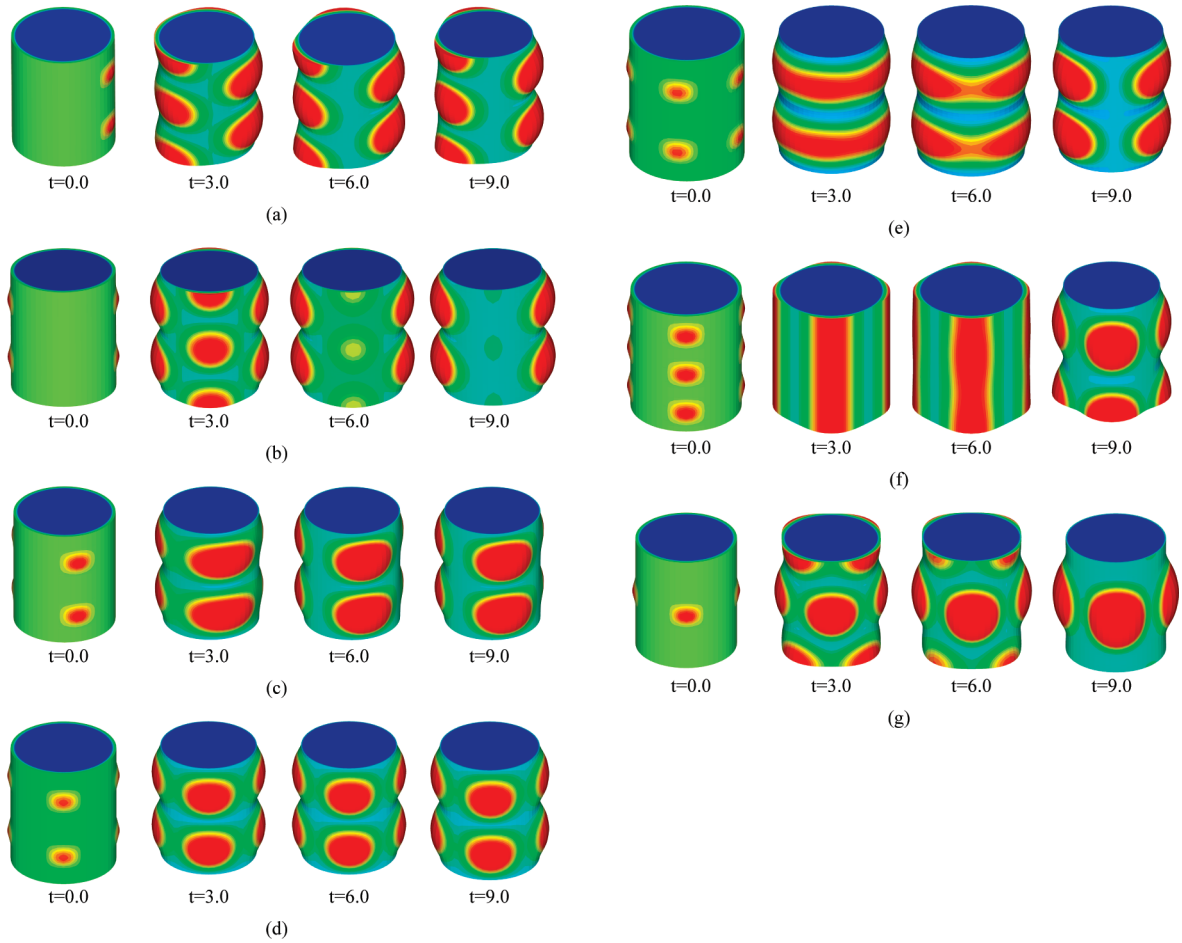

Figure 8. Morphological evolution of the prepatterned surfaces of core−shell nanowires. The shell radius is $R_s = 3.3$, the core radius $R_c = 3.0$. The size of prepatterned islands is the same, $z_0 = 1.0$ and $\theta_0 = 3\pi/8$. Pitches of the patterned islands along two directions are (a) $P_z = 4.0$ and $P_\theta = 2\pi$; (b) $P_z = 4.0$ and $P_\theta = \pi$; (c) $P_z = 4.0$ and $P_\theta = 2\pi/3$; (d) $P_z = 4.0$ and $P_\theta = \pi/2$; (e) $P_z = 4.0$ and $P_\theta = 2\pi/5$; (f) $P_z = 2.67$ and $P_\theta = \pi/2$; and (g) $P_z = 8.0$ and $P_\theta = \pi/2$.

subjected to annealing (see $t = 3.0$ in Figure 8e). These nanoring structures are in a metastable state and break up into an array of large islands when subjected to further annealing (see $t = 9.0$ in Figure 8e).

By changing the pitch along the axial direction, different island morphologies can also be obtained. A one-to-one relation can be retained when $P_z = 4.0$ and $P_\theta = \pi/2$ (see Figure 8d). For a smaller pitch in the axial direction, the prepatterned array of islands is able to join together to form nanowire structures. An example is shown in Figure 8f with $P_z = 2.67$ and $P_\theta = \pi/2$. These nanowire structures are metastable and break up into an array of large islands (see $t = 6.0$ and $t = 9.0$ in Figure 8f), which is favorable from the energetic point of view. For a larger pitch in axial direction, there is no one-to-one relation between the prepatterned islands and the formed dots at the early evolution stage. However, the newly formed islands gradually fade away when subjected to further annealing. Eventually a one-to-one-relationship is recovered. An example is shown in Figure 8g with $P_z = 8.0$ and $P_\theta = \pi/2$. The above prepatterning studies demonstrate that prepatterning routes can be also used to control the formation of island arrays on nanowire surfaces. By tuning the pitch distances to guide the growth, nanostructures such as quantum dot, nanowire, and nanoring arrays with desired distributions can be obtained.

CONCLUSIONS

In summary, going beyond the first-order instability analysis, we have performed three-dimensional dynamical simulations to understand the growth of quantum structures in core−shell nanowires. We have found that the patterns of initial perturbations have pronounced influence not only on the morphological evolution at the early stages of evolution but also on the subsequent formation and arrangement of islands. The present work suggests several possible ways to control the island array distribution, size, and density. By prepatterning initial configuration of surfaces, various nanostructures were obtained, ranging from ring arrays, dot arrays, nanowire arrays, and helical arrays. In addition, the island array stability can be maintained by prepatterning or controlling the metastable states with a capping layer. Furthermore, by controlling the outer radius of the core−shell nanowire, the island density per unit length along the nanowire axis can be changed: with increasing radius of the nanowire, the island density per unit length can be increased (for example, compare Figure 5 and Figure 6).

METHODS

First-Order Perturbation Analysis. Following the previous perturbation analysis,[21,22] the perturbation of the radius of the core−shell nanowire takes the form of $R = R_s + \delta\cos(qz)\cos(n\phi)$, where R_s is the unperturbed outer shell radius, q is the wavenumber in the axial direction, and n is the wavenumber in the circumferential direction. The growth of these perturbations is determined by stability factor:[22]

$$S = \left(\frac{n^2}{R_s^2} + q^2\right)\left(\frac{1 - n^2}{R_s^2} - q^2 - \frac{\Delta\omega}{\gamma}\right) \quad (1)$$

where $\Delta\omega$ is the change of the surface strain energy due to a sinusoidal perturbation of wavenumbers n and q. If the stability factor $S > 0$, then the initial perturbation is unstable, or it will grow with time; while if $S < 0$, the initial perturbation will decay with time.

Evolution of Surface Morphology. To simulate morphological evolution of a strained core−shell system subjected to annealing, we adopt the finite element framework developed to study the formation of quantum dots in epitaxial thin films.[31−33] In this approach, the evolution of the surface morphology is driven by the gradient of the surface chemical potential:

$$v_n = D\nabla_s^2\mu \quad (2)$$

where v_n is the surface normal velocity, $D = D_s\delta_s/k_BT$, D_s is the surface diffusion coefficient, where δ_s the diffusive layer thickness, k_B the Boltzmann constant, and T the absolute temperature. The chemical potential μ can be written as

$$\mu = \mu_0 + \Omega\left[\omega - \kappa(\gamma + W) + n_z\frac{dW}{dh}\right] \quad (3)$$

where, μ_0 is the reference chemical potential, Ω is the atomic volume of a diffusing atom, ω is the strain energy density at shell surface, γ is the surface energy of shell material, κ is the mean curvature, and $W(h)$ is the intermolecular interaction energy between core and shell, or the wetting energy. This term accounts for the presence of wetting layer observed in heteroepitaxial systems.[34,35] Here, $W(h) = B/h$, where h is the film thickness and B a material parameter ($B = h_{cr}(1 + \nu)^2\omega_0^2/\gamma$, where $\omega_0 = E\varepsilon_m^2/(1 - \nu)$ is the strain energy density for flat biaxial strained thin film, and h_{cr} the critical thickness of the wetting layer).

An isotropic linear elastic relation between strain and stress is assumed to determine the distribution of strain energy in the core−shell system. One can use the displacement field $u_i(x_j)$ of material points from stress free reference configuration of the system to describe the deformation caused by mechanical loading of the misfit strain, thus the strain due to the displacement field is $\varepsilon_{ij} = 1/2(u_{i,j} + u_{j,i})$, where the comma denotes partial differentiation with respect to a spatial coordinate. Then, the stress field related to the strains is given by

$$\sigma_{ij} = 2\mu\left[\varepsilon_{ij} - \varepsilon_m\delta_{ij} + \frac{\nu}{1 - 2\nu}(\varepsilon_{kk} - 3\varepsilon_m)\delta_{ij}\right] \quad (4)$$

where μ and ν denote shear modulus and Poisson's ratio, and ε_m is the misfit strain. The displacement and stress fields $u_i(x_j)$ and σ_{ij} can be calculated using a standard finite element method by solving the equations of mechanical equilibrium

$$\int_R \sigma_{ij}\delta u_{ij}dV = \int_{\partial R} t_i\delta u_i dA \quad (5)$$

where surface tractions $t_i = \sigma_{ij}n_j$ and n_j denotes the boundary surface normal directions.

The strain energy density is thus evaluated by $\omega = \sigma_{ij}\varepsilon_{ij}/2$. Compared to the first-order perturbation analysis, which is only suitable for prescribed sinusoidal perturbations of infinitesimal amplitude, the present approach allows one to handle perturbations of arbitrary shape and amplitude. A finite element procedure is also adopted to solve the surface diffusion eq 2, and the

details are given in refs 28−30. It is noted that eq 2 can also be solved by directly substituting the evaluated surface chemical potential into it.[36−38]

Acknowledgment. V.B.S. gratefully acknowledges support from the NSF through Grants CMMI-0926178, DMS-0914648, and DMS-0854919.

Supporting Information Available: Two movies of three-dimensional dynamic simulations showing transitions between different metastable states. Movie 1 shows the evolution of surface structures with wavenumbers $n = 2$ and $q = 2$. The normalized radius of the core is 3.3, and the shell thickness is 0.3, corresponding to Figure 4b of the main text. Two metastable states were observed during the course of the simulations. Movie 2 shows the evolution of surface structures with wavenumbers $n = 0$ and $q = 2$. The normalized radius of the core is 3.3, and the shell thickness is 0.3 corresponding to Figure 4b of the main text. Four metastable states were observed during the course of the simulation. This material is available free of charge *via* the Internet at http://pubs.acs.org.

REFERENCES AND NOTES

1. Mo, Y. W.; Savage, D. E.; Swartzentruber, B. S.; Lagally, M. G. Kinetic Pathway in Stranski−Krastanov Growth of Ge on Si(001). *Phys. Rev. Lett.* **1990**, *65*, 1020–1023.
2. Nötzel, R.; Temmyo, J.; Tamamura, T. Self-Organized Growth of Strained InGaAs Quantum Disks. *Nature* **1994**, *369*, 131–133.
3. Springholz, G.; Holy, V.; Pinczolits, M.; Bauer, G. Self-Organized Growth of Three- Dimensional Quantum-Dot Crystals with Fcc-like Stacking and a Tunable Lattice Constant. *Science* **1998**, *282*, 734–737.
4. Gudiksen, M. S.; Lauhon, L. J.; Wang, J.; Smith, D. C.; Lieber, C. M. Growth of Nanowire Superlattice Structures for Nanoscale Photonics and Electronics. *Nature* **2002**, *415*, 617–620.
5. Lauhon, L. J.; Gudiksen, M. S.; Wang, D.; Lieber, C. M. Epitaxial Core−Shell and Core−Multishell Nanowire Heterostructures. *Nature* **2002**, *420*, 57–60.
6. Cui, Y.; Zhong, Z.; Wang, D.; Wang, W. U.; Lieber, C. M. High Performance Silicon Nanowire Field Effect Transistors. *Nano Lett.* **2003**, *3*, 149–152.
7. Cui, L. F.; Ruffo, R.; Chan, C. K.; Peng, H.; Cui, Y. Crystalline-Amorphous Core−Shell Silicon Nanowires for High Capacity and High Current Battery Electrodes. *Nano Lett.* **2009**, *9*, 491–495.
8. Patolsky, F.; Lieber, C. M. Nanowire Nanosensors. *Mater. Today* **2005**, *8*, 20–28.
9. Asaro, R. J.; Tiller, W. A. Interface Morphology Development during Stress Corrosion Cracking: Part I. *via* Surface Diffusion. *Metall. Trans.* **1972**, *3*, 1789–1796.
10. Grinfeld, M. A. Instability of the Separation Boundry between a Nonhydrostatically Stressed Elastic Body and a Melt. *Sov. Phys. Dokl.* **1986**, *31*, 831–835.
11. Srolovitz, D. J. On the Stability of Surfaces of Stressed Solids. *Acta Metall.* **1989**, *37*, 621–625.
12. Gao, H.; Nix, W. D. Surface Roughening of Heteroepitaxial Thin Films. *Annu. Rev. Mater. Sci.* **1999**, *29*, 173–209.
13. Voorhees, P. W.; Davis, S. H. Morphological Instability in Epitaxially Strained Dislocation-Free Solid Films. *Phys. Rev. Lett.* **1991**, *67*, 3696–3699.
14. Petroff, P. M.; DenBaars, S. P. MBE and MOCVD Growth and Properties of Self-Assembling Quantum Dot Arrays in III−V Semiconductor Structures. *Superlattices Microstruct.* **1994**, *15*, 15–21.
15. Walther, T.; Cullis, A. G.; Norris, D. J.; Hopkinson, M. Nature of the Stranski−Krastanow Transition during Epitaxy of InGaAs on GaAs. *Phys. Rev. Lett.* **2001**, *86*, 2381–2384.
16. Mano, T.; Fujioka, H.; Ono, K.; Watanabe, Y.; Oshima, M. InAs Nanocrystal Growth on Si(100). *Appl. Surf. Sci.* **1998**, *130−132*, 760–764.
17. Pan, L.; Lew, K. K.; Redwing, J. M.; Dickey, E. C. Stranski−Krastanow Growth of Germanium on Silicon Nanowires. *Nano Lett.* **2005**, *5*, 1081–1085.
18. Goldthorpe, I. A.; Marshall, A. F.; Mclntyre, P. C. Synthesis and Strain Relaxation of Ge-Core/Si-Shell Nanowire Arrays. *Nano Lett.* **2008**, *8*, 4081–4086.
19. Tian, B. Z.; Zheng, X. L.; Kempa, T. J.; Fang, Y.; Yu, N. F.; Yu, G. H.; Huang, J. L.; Lieber, C. M. Coaxial Silicon Nanowires as Solar Cells and Nanoelectronic Power Sources. *Nature* **2007**, *449*, 885–889.
20. Huang, M; Ritz, C. S.; Novakovic, B.; Yu, D. C.; Zhang, Y.; Flack, F.; Savage, D. E.; Evans, P. G.; Knezevic, I.; Liu, F.; *et al.* Mechano-Electronic Superlattices in Silicon Nanoribbons. *ACS Nano* **2009**, *3*, 721–727.
21. Schmidt, V.; Mclntyre, P. C.; Gösele, U. Morphological Instability of Misfit-Strained Core−Shell Nanowires. *Phys. Rev. B* **2008**, *77*, 235302-1–235302-12.
22. Wang, H.; Upmanyu, M.; Ciobanu, C. V. Morphology of Epitaxial Core−Shell Nanowires. *Nano Lett.* **2008**, *8*, 4305–4311.
23. Pistol, M.-E.; Pryor, C. E. Band Structure of Core−Shell Semiconductor Nanowires. *Phys. Rev. B* **2008**, *78*, 115319-1–115319-12.
24. Montazeri, M.; Fickenscher, M.; Smith, L. M.; Jackson, H. E.; Yarrison-Rice, J.; Kang, J. H.; Gao, Q.; Tan, H. H.; Jagadish, C.; Guo, Y. N.; *et al.* Direct Measure of Strain and Electronic Structure in GaAs/GaP Core−Shell Nanowires. *Nano Lett.* **2010**, *10*, 880–886.
25. Qiao, Y. H.; Wang, D.; Buriak, J. M. Block Copolymer Templated Etching on Silicon. *Nano Lett.* **2007**, *7*, 464–469.
26. Chai, J; Buriak, J. M. Using Cylindrical Domains of Block Copolymers To Self-Assemble and Align Metallic Nanowires. *ACS Nano* **2008**, *2*, 489–501.
27. Chen, G.; Lichtenberger, H.; Schaffler, F.; Bauer, G.; Jantsch, W. Geometry Dependent Nucleation Mechanism for SiGe Islands Grown on Pit-Patterned Si(001) Substrates. *Mater. Sci. Eng., C* **2006**, *26*, 795–799.
28. Zhong, Z. Y.; Halilovic, A.; Fromherz, T.; Schaffler, F.; Bauer, G. Two-Dimensional Periodic Positioning of Self-Assembled Ge Islands on Prepatterned Si (001) Substrates. *Appl. Phys. Lett.* **2003**, *82*, 4779–4781.
29. Schmidt, O. G.; Kiravittaya, S.; Nakamura, Y.; Heidemeyer, H.; Songmuang, R.; Muller, C.; Jin-Phillipp, N. Y.; Eberl, K.; Wawra, H.; Christiansen, S.; *et al.* Self-Assembled Semiconductor Nanostructures: Climbing up the Ladder of Order. *Surf. Sci.* **2002**, *514*, 10–18.
30. Pires, D.; Hedrick, J. L.; Silva, A. D.; Frommer, J.; Gotsmann, B.; Wolf, H.; Despont, M.; Duerig, U.; Knoll, A. W. Nanoscale Three-Dimensional Patterning of Molecular Resists by Scanning Probes. *Science* **2010**, *328*, 732–735.
31. Zhang, Y. W.; Bower, A. F. Numerical Simulations of Island Formation in a Coherent Strained Epitaxial Thin Film System. *J. Mech. Phys. Solids* **1999**, *47*, 2273–2297.
32. Zhang, Y. W.; Bower, A. F.; Liu, P. Morphological Evolution Driven by Strain Induced Surface Diffusion. *Thin Solid Films* **2003**, *424*, 9–14.
33. Liu, P.; Zhang, Y. W.; Lu, C. Computer Simulations of the Stranski−Krastanov Growth of Heteroepitaxial Films with Elastic Anisotropy. *Surf. Sci.* **2003**, *526*, 375–382.
34. Tu, Y.; Tersoff, J. Origin of Apparent Critical Thickness for Island Formation in Heteroepitaxy. *Phys. Rev. Lett.* **2004**, *93*, 216101-1–216101-4.
35. Suo, Z.; Zhang, Z. Epitaxial Films Stabilized by Long-Range Forces. *Phys. Rev. B* **1998**, *58*, 5116–5120.
36. Chiu, C.-H. Stable and Uniform Arrays of Self-Assembled Nanocrystalline Islands. *Phys. Rev. B* **2004**, *69*, 165413-1–165413-4.
37. Ramasubramaniam, A.; Shenoy, V. B. Three-Dimensional Simulations of Self-Assembly of Hut-Shaped Si−Ge Quantum Dots. *J. Appl. Phys.* **2004**, *95*, 7813–7821.
38. Chiu, C. -H.; Huang, Z. Numerical Simulation for the Formation of Nanostructures on the Stranski−Krastanow Systems by Surface Undulation. *J. Appl. Phys.* **2007**, *101*, 113540-1–113540-10.